Int. J. Multiphase Flow Vol. 11, No. 3, pp. 299–315, 1985
Printed in the U.S.A.

0801–9322/85 $3.00 + .00

EMPIRICAL EQUATIONS TO PREDICT FLOW PATTERNS IN TWO-PHASE INCLINED FLOW

HEMANTA MUKHERJEE
Flopetrol-Johnston Schlumberger, Anchorage, AK 99511, U.S.A.

and

JAMES P. BRILL
The University of Tulsa, Tulsa, OK 74104, U.S.A.

(*Received* 15 *March* 1982; *in revised form* 19 *September* 1984)

Abstract—Based on experimental data, flow regime maps were drawn for different inclination angles, including horizontal and vertical flow. Different empirical equations for the flow regime transitions are proposed that are functions of inclination angle for both upflow and downflow. In general, the flow regimes and their transitions for upflow were similar to those proposed by Duns and Ros for vertical upflow. For downflow, the flow regimes and their transitions conformed more to the Mandhane *et al.* type of flow regime map. The stratified flow region in downflow was found to be affected appreciably by the angle of inclination. A detailed comparison of the proposed transition equations with a number of flow regime maps is also presented.

INTRODUCTION

One of the most important aspects of two-phase flow in pipes is the geometric distribution of the two phases under flowing conditions. This geometric distribution is often termed flow regime or flow pattern. The flow regime in two-phase flow depends on the pipe angle and flow direction together with other flow and fluid parameters. The present state of the art lacks information regarding flow pattern transitions and their functional relationships with angle of inclination for either upflow or downflow. Extensive research has been conducted on understanding and prediction of the flow regime transitions in two-phase flow for limited ranges of inclination angle. The published work can be classified into empirical and analytical categories. Empirical flow pattern maps are those in which the flow pattern transitions are defined from visual observations and plotted with a set of independent variables uniquely defining the flow patterns. Subjectivity in the flow pattern definition, improper experimental design, and natural inconsistencies in the perception of flow patterns often lead to a wide transition band. A mathematical definition of flow pattern transitions requires the fitting of the best single curve through this wide band. Analytical flow pattern predictions, on the other hand, are based on the physical forces responsible for the geometric distribution of the phases.

There are a number of flow pattern maps available in the literature. Most of these are for horizontal flow or vertical upflow. Among the many horizontal flow pattern maps published, a revision of the Govier & Omer (1962) map proposed by Mandhane *et al.* (1974) is quite extensively used. In vertical upflow, the most significant flow pattern maps were proposed by Griffith & Wallis (1961), Duns & Ros (1963), Govier & Aziz (1972) and Oshinowo & Charles (1974). These flow pattern maps differ considerably from each other. The extent of differences is much larger for vertical upflow than for horizontal flow. An important reason for the discrepancies in vertical upflow maps is the inconsistency in the dimensionless groups forming the independent mapping variables.

Unlike horizontal flow, gravity effects dominate the flow pattern transitions in vertical upflow. Because of high liquid holdup, this is especially true for the bubble–slug transitions. The relative contribution of gravity forces compared to inertial forces may be quite

significant at the lower gas rates required for bubble–slug transition. The slug–annular mist transition, on the other hand, is so dominated by the high gas velocities that gravity effects are rendered insignificant. This could result in a shift in the bubble–slug transition for liquids having different densities if the coordinates selected do not properly account for density changes.

For inclined two-phase flow, there have been no attempts to empirically correlate flow pattern transitions as a function of inclination angle. Gould *et al.* (1974) observed flow patterns for horizontal, vertical and 45° upflow. They used the Duns and Ros coordinates to plot their flow pattern maps. Their flow patterns were defined similar to those of Duns & Ros with one additional flow pattern of both phases continuous in upflow. Taitel & Dukler (1976) proposed a model for predicting flow pattern transitions in horizontal and near-horizontal gas–liquid flow. Starting with stratified flow, the mechanisms by which a change from stratified flow can result were studied. From the physical concepts of the flow pattern transitions, different mathematical criteria for these transitions from stratified flow were formulated. These criteria were dependent on solutions to a two-phase momentum balance equation for stratified flow. Recently, Taitel *et al.* (1980) also published models for predicting flow pattern transitions during steady gas–liquid upflow in vertical pipes, and Barnea *et al.* (1982) described flow pattern transitions for vertical downflow and for downward inclined flow.

The purpose of this study was to develop an empirical method to predict flow patterns in pipe at all possible inclination angles. Following sections describe the experimental program, inclined flow pattern transitions, the empirical equations developed to predict transitions and compare the equations with selected existing flow pattern maps to validate the equations.

EXPERIMENTAL EQUIPMENT AND TESTING PROCEDURE

The test section consists of an inverted, U-shaped, 3.81 cm nominal ID steel pipe. Each leg of this U is 17 m long, with 6.71 m entrance lengths followed by 9.75 m long test sections on both upflow and downflow sides. Each of these test sections can be isolated from the rest of the piping by pneumatically actuated ball valves that can be opened or closed simultaneously with a three-way switch. The test sections are provided with two pressure taps 9.30 m apart as shown in figure 1. Near the center of these 9.75 m long sections, there are two 2.13 m long transparent lexan pipe sections to permit visual observation of flow patterns for both upflow and downflow. These electrically insulating sections also contain capacitance type holdup sensor elements discussed by Mukherjee (1979). The oil and gas phases are metered and then allowed to mix in a mixing tee. After flowing through a 12.192 m section of 5.08 cm ID pipe, the two-phase mixture enters the test loop through a flexible hose. On the outlet side of the test loop, the two-phase mixture enters a horizontal separator through another 12.192 m long, 5.08 cm ID smooth hose and a length of about 9.144 m of 5.08 cm ID steel pipe. Long, smooth, flexible hoses are used to help minimize the entrance and exit effects. The closed end of the U-shaped test loop can be raised or lowered to any angle from 0°–90° with the help of an electric winch and a system of block and tackle pulleys hung from a small beam on top of a 21.336 m high tower. The liquid flow rates were measured by two turbine meters of different flow ranges. Very low liquid flow rates were measured with a rotameter. The flow rates from the turbine meters could be controlled manually by a globe valve or automatically by a flow control system.

The compressed air supply was provided by a two-stage compressor with a maximum rated capacity of 20 MSCM/D at 9.3 bar discharge pressure. A pressure controller was used to maintain a constant static supply pressure around 8.6 bar prior to entering the orifice meter run. The recorded pressure fluctuations were limited to 0.14 bar depending on the flow rate. The air flow was measured by one of two orifice meters or a rotameter.

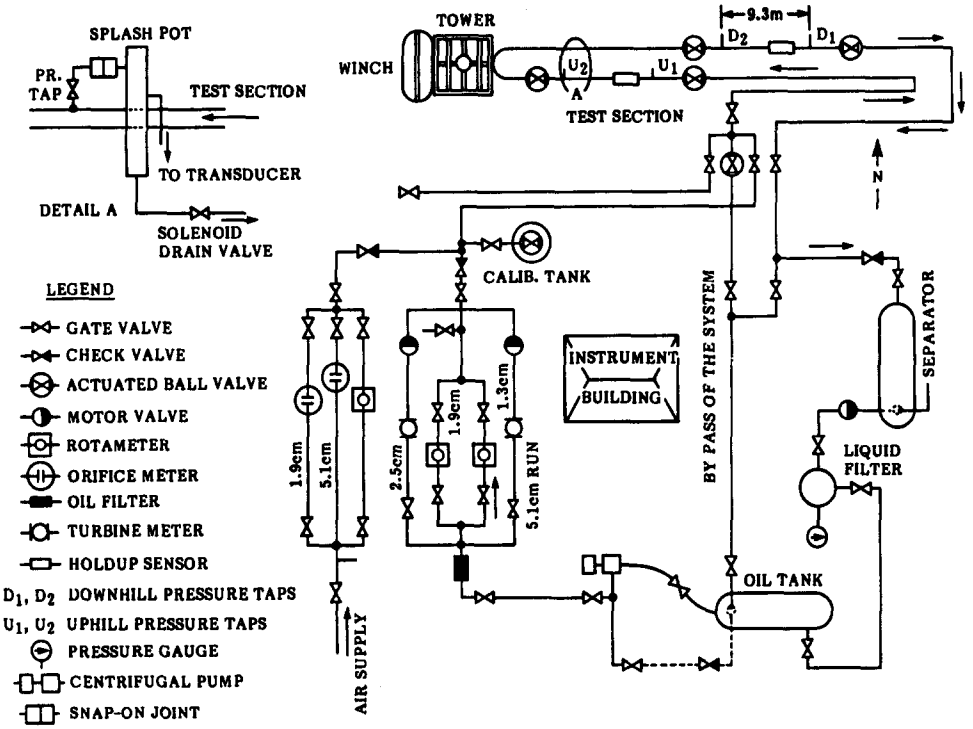

Figure 1. Schematic diagram of inclined flow experimental system.

FLUID PHYSICAL PROPERTIES

Kerosene and lubricating oil were used as the liquid phases. These oils were selected to study the effect of oil viscosity on the flow regime transitions. Compressed air was used as the gas phase. The physical properties of both liquid phases were determined from laboratory measurements for a wide range of temperatures. These data were plotted as functions of temperature and the following regression equations were fitted to the data.

Kerosene

$$\sigma = 27.6 - 0.09\,T,$$
$$\rho = 832.34 - 0.8333\,T,$$
$$\mu = 1.0E - 03 \exp(1.0664 - 0.0207\,T),$$

Lubricating Oil

$$\sigma = 36.6094 - 0.117\,T,$$
$$\rho = 861.22 - 0.7585\,T,$$
$$\mu = 1.0E - 03 \exp(3.99 - 0.0412\,T),$$

where σ is surface tension in dyne/cm, ρ is density in kg/m^3, μ is oil viscosity in Pa and T is the oil temperature in °C.

DISCUSSION OF INCLINED FLOW PATTERN TRANSITIONS

Depending on the characteristic form of the geometrical distribution of gas and liquid in the pipe, four major flow patterns were identified. Some authors prefer to subdivide these basic flow patterns into a number of subregions. Unfortunately, since a flow pattern can be very chaotic, it is very difficult to observe and objectively identify most of these subregions.

Hubbard & Dukler (1966) suggested that all of these flow patterns can be represented by the following same four basic flow patterns considered in this work: bubble; slug; stratified; and, annular mist. Characteristics of these flow patterns and transitions follow.

Bubble flow

In horizontal flow at lower liquid and gas rates, bubble flow is characterized by the formation of small discrete bubbles flowing mainly along the top of the pipe due to gravity segregation. As the liquid rate increases, the bubbles get more dispersed, ultimately forming a very homogeneous flow of uniformly distributed small gas bubbles in a continuous liquid phase, as shown in figure 2(a). As the gas flow rate is increased, the gas bubbles coalesce and grow in size, forming elongated bubble flow. In horizontal flow for high liquid rates and at a fixed gas rate depending on the liquid viscosity number, the gas bubbles grow to a limiting size, due to coalescence and expansion, before changing to slug flow. If the superficial liquid velocity is more than about 2.44 m/s, the fluid is so dispersed that it is impossible to see the transition very clearly. Below this liquid velocity in the bubble flow range, quite long (1.0 to 1.5 m) bubbles are observed before slugs are formed, as shown in figure 2(b).

When the pipe is inclined upwards, at low gas rates the small discrete gas bubbles flow through the upper part of the pipe cross section. As the gas rate is increased, the gas bubbles tend to occupy an increasing cross section of the pipe. At high gas rates, however, small gas bubbles tend to coalesce to form larger gas bubbles. At higher angles of inclination, the small gas bubbles are quite dispersed and more uniformly distributed along the cross section of the pipe. At all angles excepting vertical upflow, there is a concentration gradient of the discrete bubbles across the pipe cross section, as shown in figure 2(c). At lower angles of inclination, because of higher concentration of small gas bubbles at the top of the pipe, bubbles coalesce at lower gas rates to form larger bubbles which ultimately form slugs. As the inclination angle increases, the gas bubbles distribute over a wider cross section of the pipe, requiring a higher gas velocity to increase the gas concentration and force coalescence. Thus, at steeper

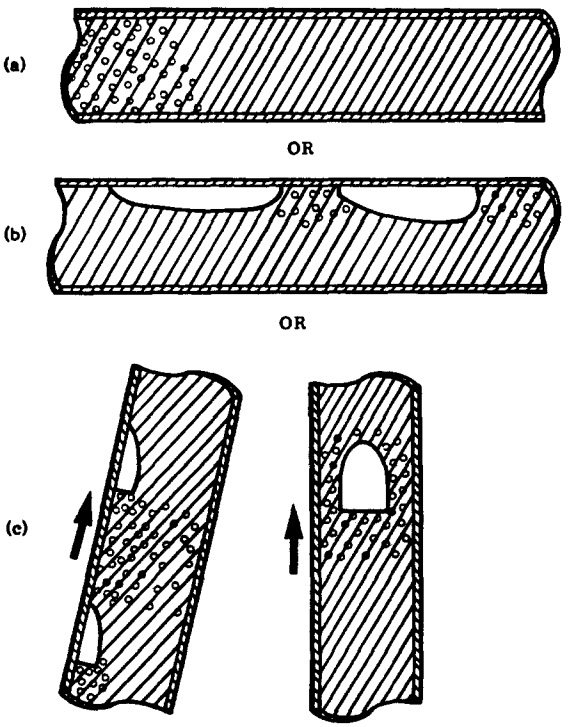

Figure 2. (a) Horizontal bubble flow. (b) Horizontal elongated bubble flow (not to scale). (c) Bubble–slug transition flow pattern for vertical and inclined upflow.

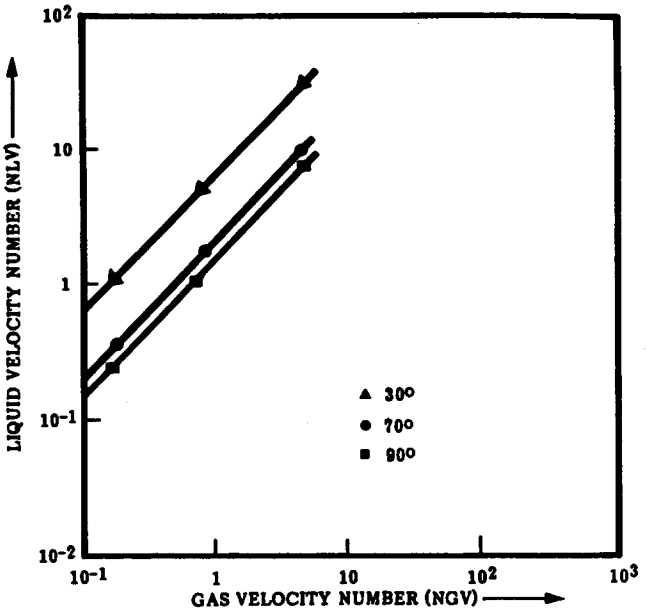

Figure 3. Predicted bubble–slug transitions for kerosene at different upflow angles.

inclination angles, it takes a higher gas velocity at a fixed liquid velocity to reach the transition from bubble-to-slug flow, as shown in figure 3.

In downflow, the bubble rise velocity component of the gas phase velocity is always countercurrent to the general flow directon. This causes collision of gas bubbles with the liquid mass, resulting in the shearing and degeneration of bubbles into smaller ones. In downflow, such collision and degeneration of bubbles cause considerable dispersion compared to upflow. This also explains the occurrence of bubble–slug transition at higher gas rates in downflow. In this case, there also is a concentration gradient of bubbles across the pipe cross section, causing the bubble–slug transition to occur at lower gas rates at lower angles above a fixed liquid velocity, as shown in figure 4. This phenomenon was observed with very carefully repeated tests in this transition region for horizontal and vertical

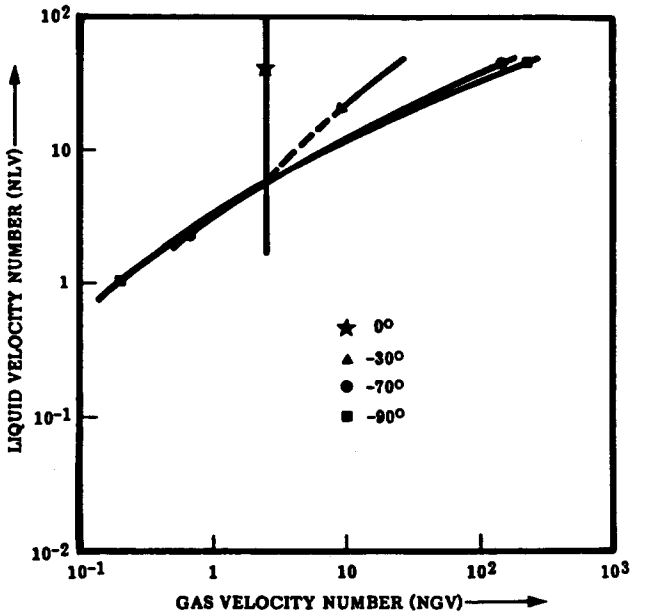

Figure 4. Predicted bubble–slug transitions for kerosene at different downflow angles.

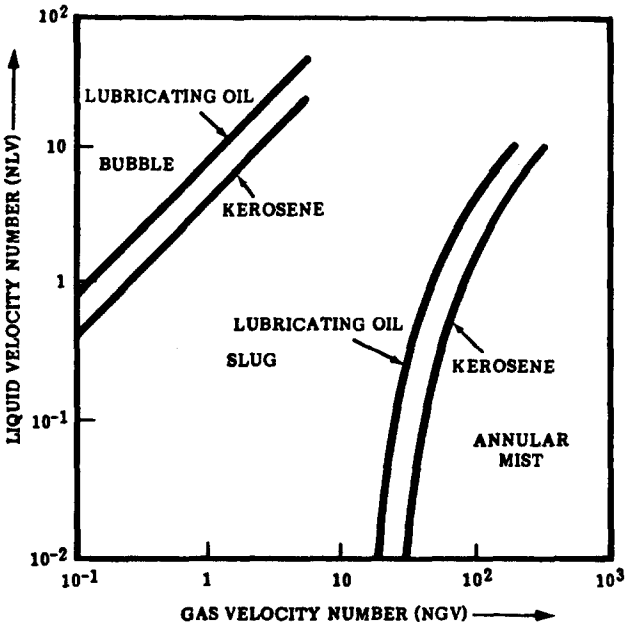

Figure 5. Effect of viscosity on flow pattern transitions—45° upflow.

downflow for both of the experimental oils. In all these cases, the bubble–slug transitions were found to intersect each other.

Liquid viscosity seems to have considerable effect on this transition for both upflow and downflow. In both these cases, higher oil viscosity (i.e., lubricating oil) causes bubble-to-slug transition at lower gas velocity numbers, as shown in figures 5 and 6. In very viscous liquids, small bubbles which have more surface area per unit volume are subjected to very high shear stresses causing large viscous drag. This slows down these bubbles, increasing the gas bubble residence time defined as the time required by a gas bubble to pass through a certain cross section of the pipe. This phenomenon continues until the bubbles coalesce and grow to a size where the surface area per unit volume is small enough to permit bubble movement at the

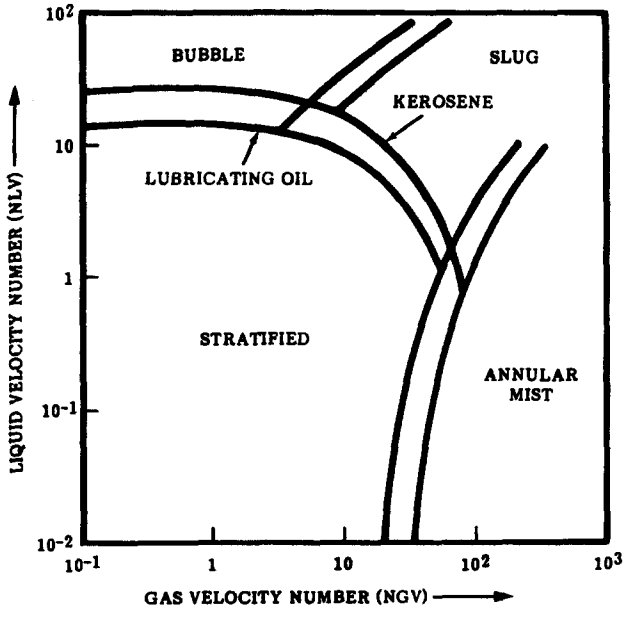

Figure 6. Effect of viscosity on flow pattern transitions—30° downflow.

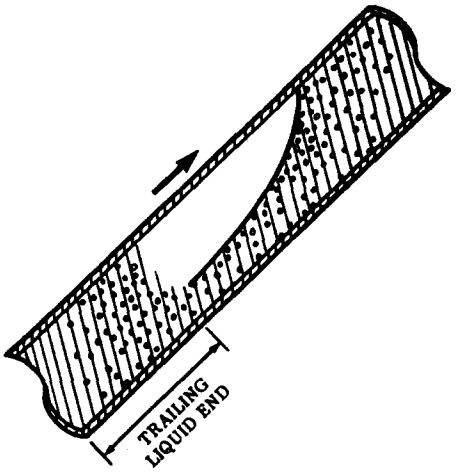

Figure 7. Typical upward inclined slug flow.

stabilized insitu velocity. Thus, higher liquid viscosity promotes formation of larger bubbles that create slugs at lower gas rates.

Slug flow

In vertical upflow, Govier & Aziz (1972) state that increasing gas rates at a constant liquid rate will eventually create cap-shaped bubbles which almost bridge the pipe, heralding the onset of slug flow. This explanation was found to be inadequate when applied to all angles of inclination and directions of flow. In horizontal flow, these cap-shaped bubbles are not seen at all. In inclined flow, onset of slugging is marked by wedge-shaped slugs, as shown in figure 7. A more versatile definition of slug flow specifies the dynamics rather than the shape or size of the gas bubble at the transition.

Near the transition from bubble to slug flow, the bubble expands in the direction of flow for the pressure gradient established. This causes liquid to accelerate in front of the gas bubble, requiring a liquid fall-back or slip-back from the rear of the bubble to maintain continuity. Thus, a trailing end is a very distinctive feature of a slug in upflow and horizontal flow, as shown in figure 7.

In downflow, slug flow was observed only at very high liquid rates. Normally, in downflow bubble flow is characterized by dispersed bubbles. Large bubbles at lower liquid rates tend to rise up the pipe due to buoyancy effects, until they coalesce to form what is called stratified flow. Slug flow occurs when the liquid rate is high enough to push the larger bubbles down the pipe with the liquid–gas mixture. Thus, when cap or wedge-shaped bubbles of about twice the pipe diameter in length are seen to flow with the superficial mixture velocity, slug flow is said to commence.

In downflow at higher liquid rates, as gas velocity is increased at a fixed liquid velocity, bubble-to-slug flow transition occurs. At lower liquid rates, figures 8 and 9 show that bubble-to-stratified flow transition occurs for inclination angles steeper than $-30°$. However, from $0°$ to $-30°$ at lower liquid rates, figures 10 and 11 show that bubble flow did not occur for the range of flow parameters considered.

Slug flow is also characterized by fluctuations in pressure and liquid holdup profiles. The frequency of these fluctuations depends on phase flow rates. The range of pressure fluctuations tends to increase with increasing gas rates almost until annual mist flow begins. Liquid holdup traces show a peak equivalent to the liquid holdup of the liquid slugs and depends on the amount of entrained gas. At higher gas rates, slug flow is very frothy, preventing a correct visual description of the slugs. However fluctuations in pressure and liquid holdup profiles are still characteristic.

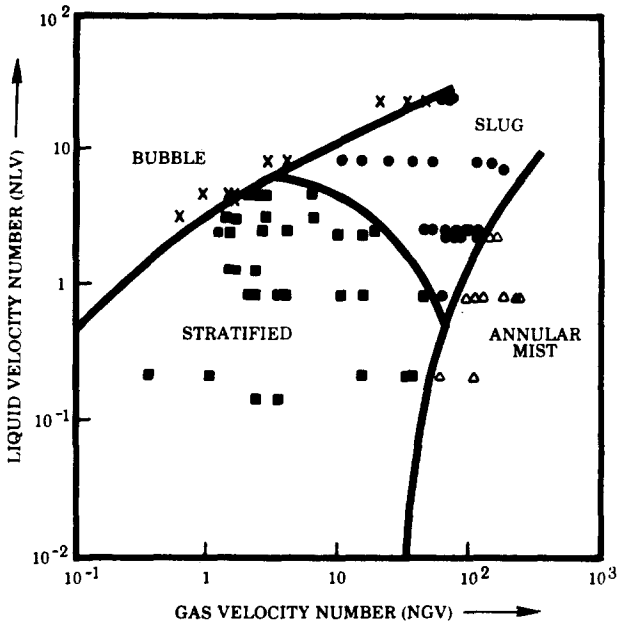

Figure 8. Comparison of experimental observations with predicted flow pattern transitions for kerosene—70° downflow.

Stratified flow

In horizontal flow and for most downflow angles, stratified flow is observed when both gas and liquid rates are low. At higher gas rates, stratified flow becomes slug flow with increasing liquid rate, and annular mist flow with decreasing liquid rates. At lower gas rates, the liquid–gas interface is smooth. As the gas rate is increased, the interface becomes wavy. The exact gas and liquid rates at which these transitions occur for the fluids used in this work can be obtained from the appropriate transition equations presented in the following section.

In the flow pattern maps shown in figures 8–11, the stratified flow envelope increases

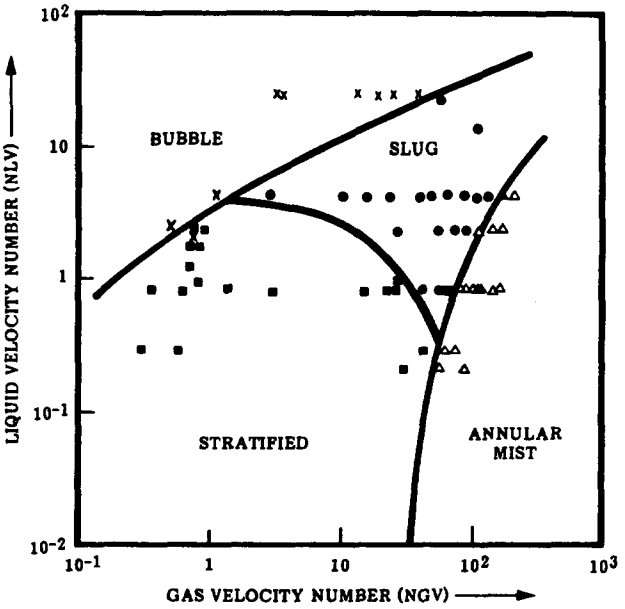

Figure 9. Comparison of experimental observations with predicted flow pattern transitions for kerosene—90° downflow.

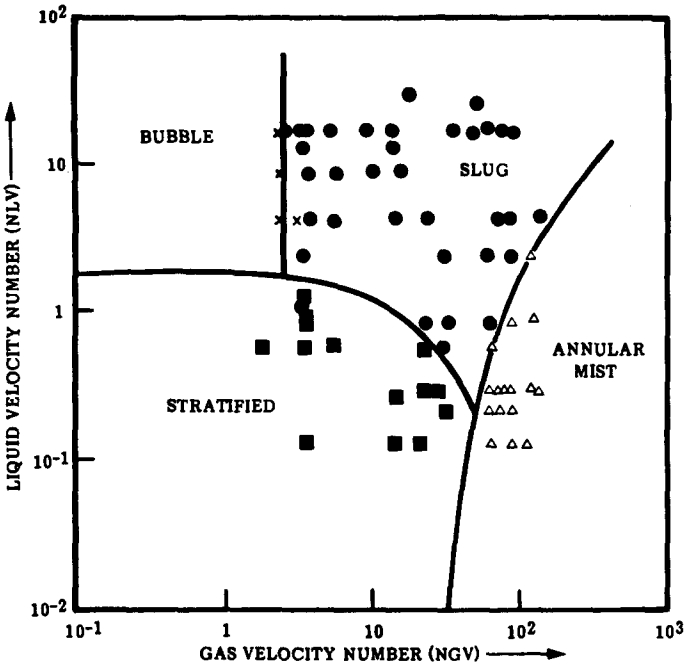

Figure 10. Comparison of experimental observations with predicted flow pattern transitions for kerosene—horizontal flow.

from 0° to −30°. With further increase in negative pipe inclination, the envelope for stratified flow shrinks. Any downflow promotes stratification at lower liquid rates. During stratified flow, a velocity gradient in the liquid strata is established from the pipe wall to the liquid–gas interface. At steeper downflow angles, this velocity gradient becomes very high and the liquid near the interface becomes turbulent. This and other causes of instabilities in the interface results in liquid splashes or waves. These waves are also enhanced by higher gas rates. Slug flow results when these waves bridge the pipe cross section. At higher liquid and lower gas rates, bubble flow may result from such instabilities. This transition creates a

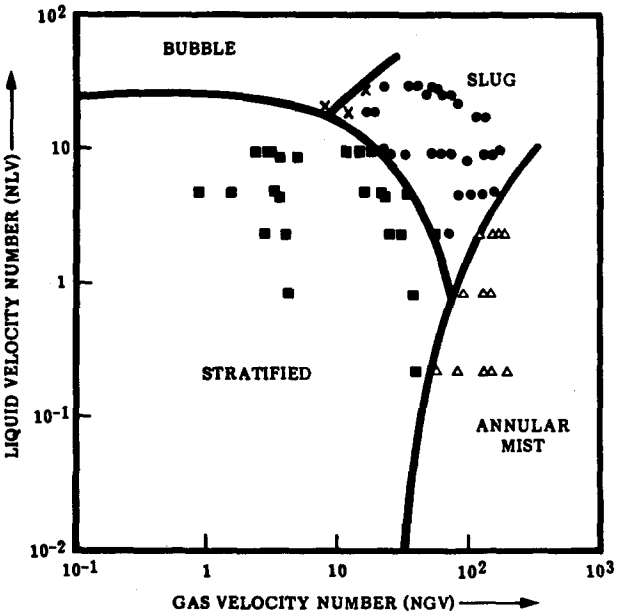

Figure 11. Comparison of experimental observations with predicted flow pattern transitions for kerosene—30° downflow.

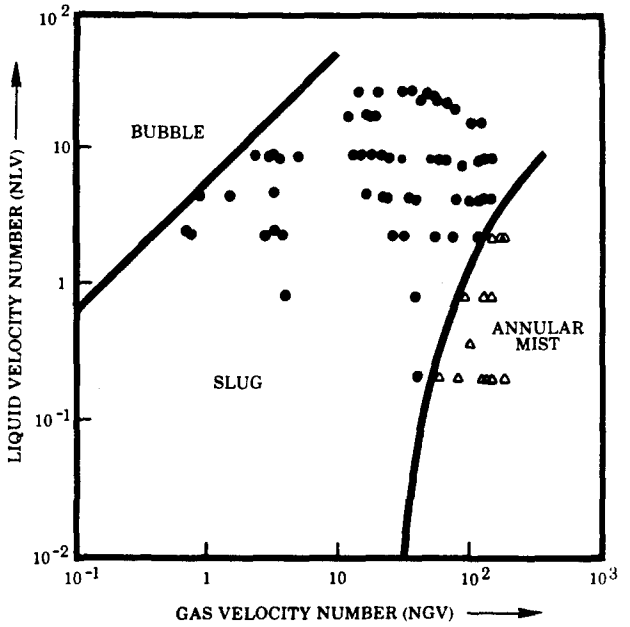

Figure 12. Comparison of experimental observations with predicted flow pattern transitions for kerosene—30° upflow.

sudden change from no pressure recovery in stratified flow to partial or full pressure recovery as it changes to bubble or slug flow.

Higher liquid viscosity seems to shrink the stratified flow envelope. Higher liquid viscosity increases the velocity gradient in the liquid layer from the pipe wall to the oil–gas interface. This causes bulged waves on the liquid surface. These bottom-heavy waves are more vulnerable to the turbulence in the gas layer, imparting instabilities on the liquid surface which can obstruct the gas flow and cause slug or bubble flow.

A type of stratified flow was observed in vertical downflow. The flow pattern here looks more like annular flow, although the flow mechanics in vertical downflow for annular and

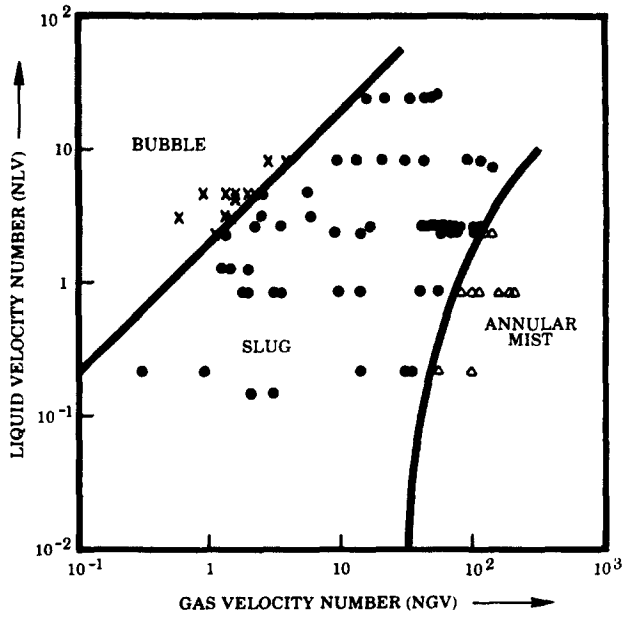

Figure 13. Comparison of experimental observations with predicted flow pattern transitions for kerosene—70° upflow.

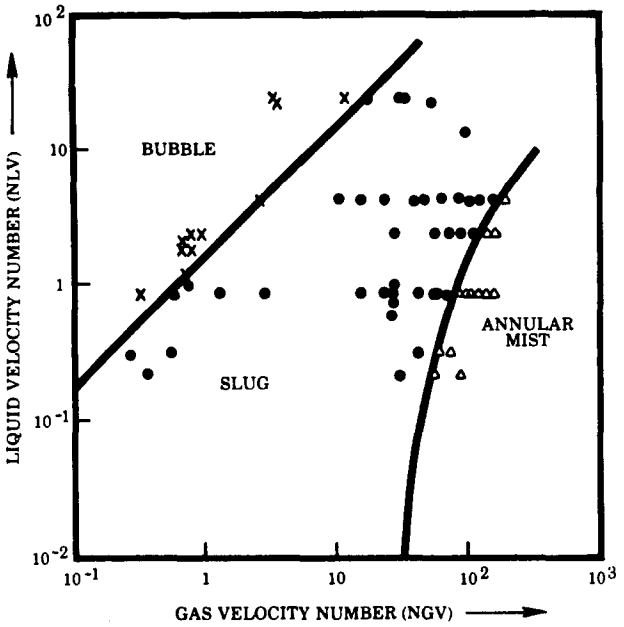

Figure 14. Comparison of experimental observations with predicted flow pattern transitions for kerosene—90° upflow.

stratified flow can be clearly separated. In the so called vertical stratified downflow, the liquid falls freely and accelerates to a very high velocity, decreasing liquid holdup substantially. In this case very little or no pressure gain is normally observed, which is similar to stratified flow at other angles. This flow pattern is also similar to stratified flow in that there is an absence of entrained liquid in the gas core. The flow pattern is identified as stratified flow in the empirical flow pattern envelopes presented. Figures 12–14 show that stratified flow was not observed for any of the upflow angles considered.

Annular mist flow

At all pipe inclinations in both upflow and downflow, as the gas flow rate is increased at a fixed liquid flow rate, annular flow is eventually observed. The gas flow rate for a fixed liquid

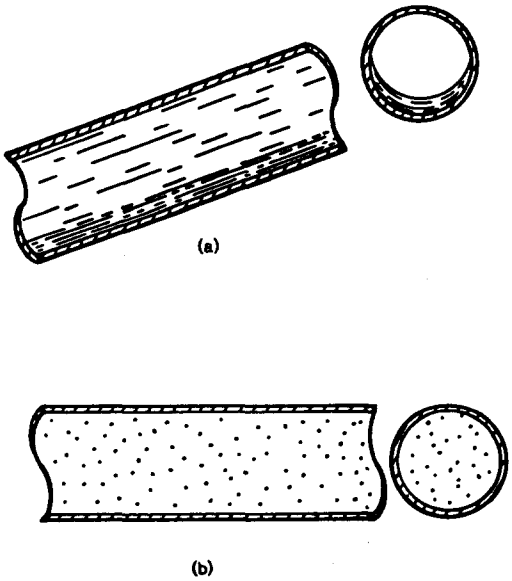

Figure 15. (a) Inclined annular mist flow. (b) Total mist flow.

flow rate at which annular flow starts is called the transition gas flow rate for that liquid rate. In annular flow, the gas phase becomes continuous along the pipe core. The continuous gas core is eccentric or concentric in the pipe, depending on the inclination of the pipe. In vertical flow, the gas core is normally concentric. This flow pattern is further characterized by the near absence of slippage. A typical flow cross section is shown in figure 15(a). At very high gas rates, all the liquid tends to be entrained in the gas core as small droplets or mist, as shown in figure 15(b). Mist flow begins when the no-slip holdup is approximately 1% or less.

EMPIRICAL FLOW PATTERN TRANSITION EQUATIONS

For each oil, observed flow pattern maps were drawn on log–log scales with dimensionless gas and liquid velocity numbers as the coordinates. The transition curves were drawn on each map. These curves were then fitted with nonlinear regression equations using a Biomedical Computer Program (BMDP 1977).

Two transitions were fitted for upflow. The bubble–slug transition was found to be linear and at 45° with the axis. The equation of these sets of straight lines was found to be

$$N_{Lv\text{BS}} = 10^{**}\,[\log_{10}(N_{Gv}) + 0.940 + 0.074\sin\theta - 0.855\sin^2\theta + 3.695\,N_L], \qquad [1]$$

where the dimensionless numbers for any set of consistent units were defined as

$$N_{Lv} = v_{\text{SL}}\sqrt[4]{\frac{\rho_L}{g\sigma}},$$

$$N_{Gv} = v_{\text{SG}}\sqrt[4]{\frac{\rho_L}{g\sigma}},$$

$$N_L = \mu_L\sqrt[4]{\frac{g}{\rho_L\sigma^3}},$$

v_{SL} = superficial liquid velocity,

v_{SG} = superficial gas velocity,

θ = inclination angle from horizontal (+ = upflow).

The slug–annular mist transition was found to be identical for horizontal and all upflow and downflow angles. However, liquid viscosity was found to have a significant effect on this transition. Increased liquid viscosity accelerates the transition from slug to annular mist flow. The equation of this transition curve was

$$N_{Gv\text{SM}} = 10^{**}\,(1.401 - 2.694\,N_L + 0.521\,N_{Lv}^{0.329}). \qquad [2]$$

In downflow and horizontal flow, the equation for the bubble–slug transition was found to be

$$N_{Gv\text{BS}} = 10^{**}\,[0.431 + 1.132\sin\theta - 3.003\,N_L - 1.138\,(\log_{10}N_{Lv})\sin 0 - 0.429\,(\log_{10}N_{Lv})^2\sin\theta] \qquad [3]$$

This transition generates a family of curves for different angles of inclination and liquid viscosities. In horizontal flow, this transition becomes a function of viscosity only, and is a vertical straight line.

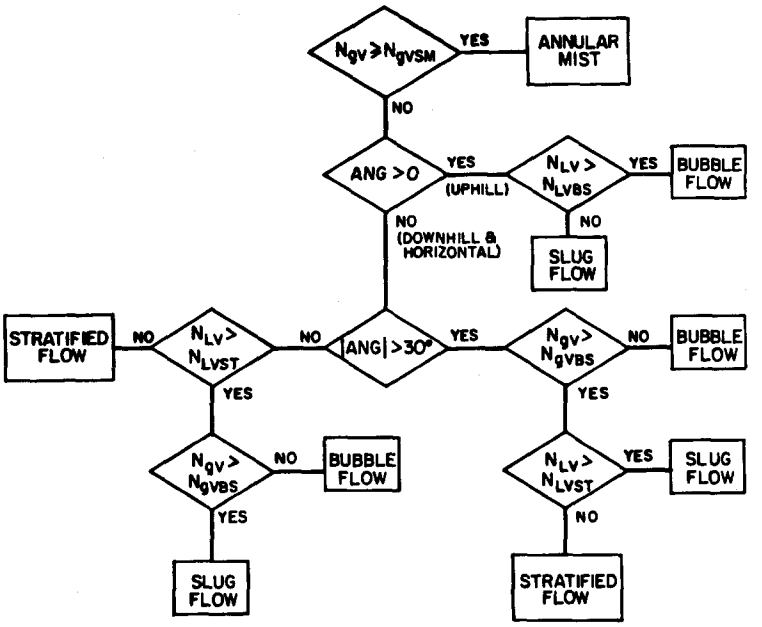

Figure 16. Flow chart for determining flow pattern transitions.

The downflow and horizontal stratified flow boundary is given by the equation

$$N_{L/ST} = 10^{**}\,[0.321 - 0.017\,Ngv - 4.267 \sin\theta - 2.972\,N_L - 0.033\,(\log_{10} Ngv)^2 - 3.925 \sin^2\theta] \quad [4]$$

In downflow at higher liquid rates, as gas velocities increase at a fixed liquid velocity, bubble-to-slug flow transition occurs. At lower liquid rates, bubble-to-stratified flow transition occurs below inclination angles of $-30°$. However, from $0°$ to $-30°$ at lower liquid rates, bubble flow did not occur for the range of flow parameters considered.

A flow chart for predicting flow pattern using the above flow pattern transition equations appears in figure 16. Note that the subscripts BS, SM and ST in [1]–[4] and figure 16 represent the bubble–slug, slug–annular mist and stratified transitions, respectively.

Comparisons of data with transition curves based on the regression equations are shown in figures 8–14 for kerosene and air. The accuracy of the regression equations appears to be excellent.

COMPARISON OF PREDICTIONS WITH EXISTING FLOW PATTERN MAPS

The flow pattern transition equations can be used to generate flow pattern maps with a variety of coordinates. Maps were generated with the identical coordinates used for published maps for vertical upflow, 45° upflow and horizontal flow.

In vertical upflow, flow pattern transition equations for kerosene at 294 K are compared with the Duns & Ros (1963) map in figure 17. The proposed bubble–slug transition from [3] occurs at a lower gas velocity number than given by Duns and Ros. However, this transition is almost identical to that in the Schmidt *et al.* (1981) map which predicts a parallel line slightly to the left of the proposed transition. The difference in these lines is negligible considering the subjective nature of transition identification. The slug–annular mist transition prediction by [2] is identical to the slug–transition boundary in the Duns and Ros map. The Schmidt map predicts the slug–annular mist transition to occur at lower gas velocity numbers.

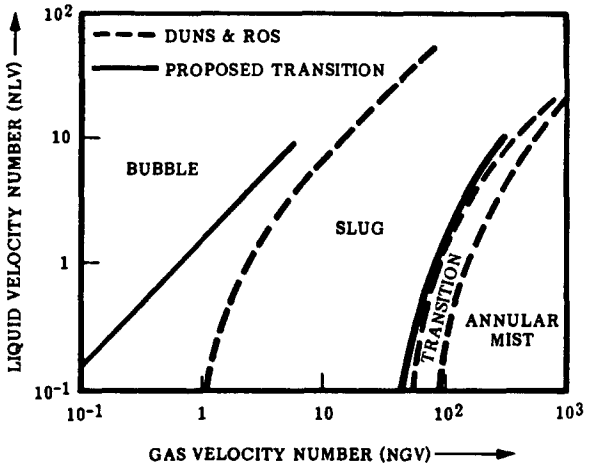

Figure 17. Comparison of proposed flow pattern transition equations with Duns and Ros map—vertical upflow.

Figures 18–20 compare the Gould *et al.* (1974) flow regime transitions for vertical upflow, 45° upflow and horizontal flow with the corresponding transitions predicted by [1]–[4]. Gould *et al.* used tap water for their liquid phase. They identified four flow regimes as liquid phase continuous, alternating phases, gas phase continuous and both phases continuous. These are equivalent to the bubble, slug, annular and stratified flow regimes. Figure 18 shows that, for vertical upflow, the bubble–slug transition predicted by [1] occurs at a higher gas velocity number for any fixed liquid velocity number than the Gould *et al.* bubble–slug transition band. Hence, the proposed bubble–slug transition lies between those of Duns and Ros and Gould *et al.* Taitel *et al.* (1980) compared their bubble–slug transition from physical modeling with those of seven published vertical upflow flow pattern maps. They concluded that all these transitions fall on a band bounded by the Gould *et al.* and Duns and Ros transitions. A further investigation of this transition shows that both [1] and the Taitel *et al.* model predict this transition to pass through the center of this band.

Gould *et al.* also report a both-phases continuous zone in their upflow maps which is not observed in the present work. Also, the transition from slug to annular mist predicted by [2]

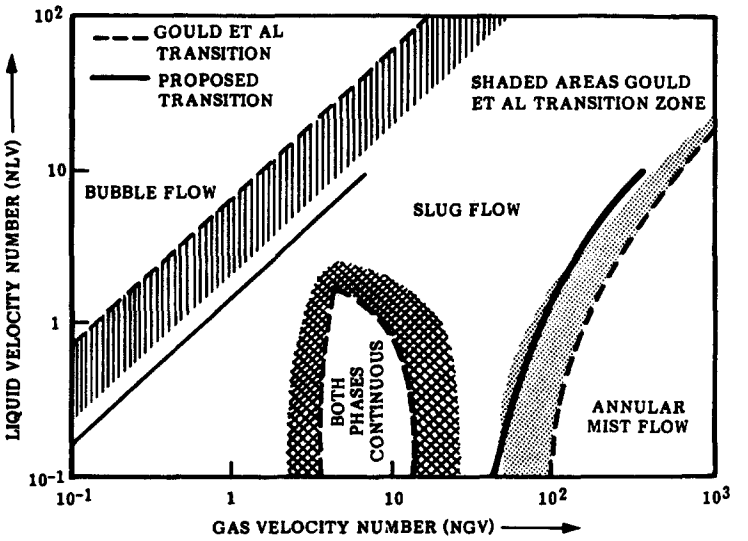

Figure 18. Comparison of proposed flow pattern transition equations with Gould *et al.* map—vertical upflow.

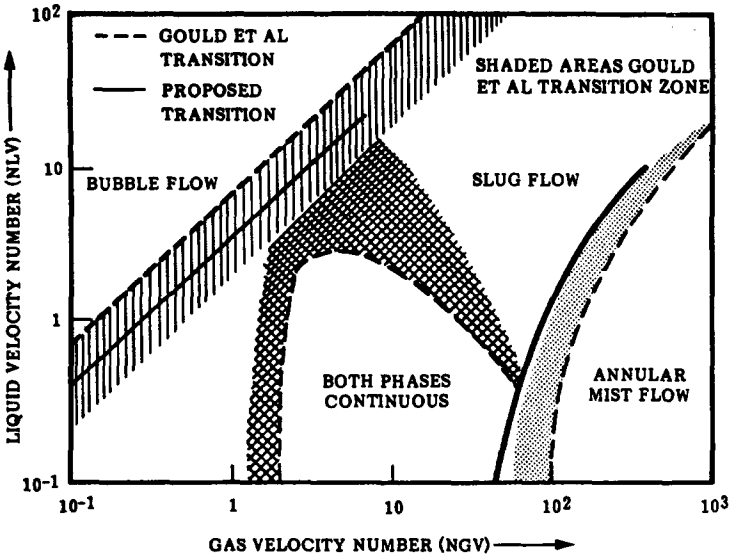

Figure 19. Comparison of proposed flow pattern transition equations with Gould *et al.* map—45° upflow.

occurs at a lower gas velocity number than in the Gould *et al.* map. Taitel *et al.* studied this transition and compared their model to eight published maps. They conclude that both the Duns and Ros and Gould *et al.* maps predict this transition at higher gas velocity numbers. Hence, based on this study, the predicted slug–annular mist transition is compatible with the published literature.

Figure 19 shows a comparison of predictions with the Gould *et al.* map for 45° upflow. The predicted bubble–slug boundary lies at the center of the Gould transition band. The slug–annular mist boundary almost overlies the slug-transition boundary of the Gould map. The both-phases continuous regime (i.e. stratified flow) was not observed in this study.

The horizontal flow pattern map in figure 20 shows good agreement for the stratified flow envelope as predicted by [4]. However, the predicted bubble–slug transitions intersect each other. At higher liquid velocity numbers, the Gould *et al.* map will predict this transition at a higher gas velocity number than that predicted by [3]. At lower liquid velocity

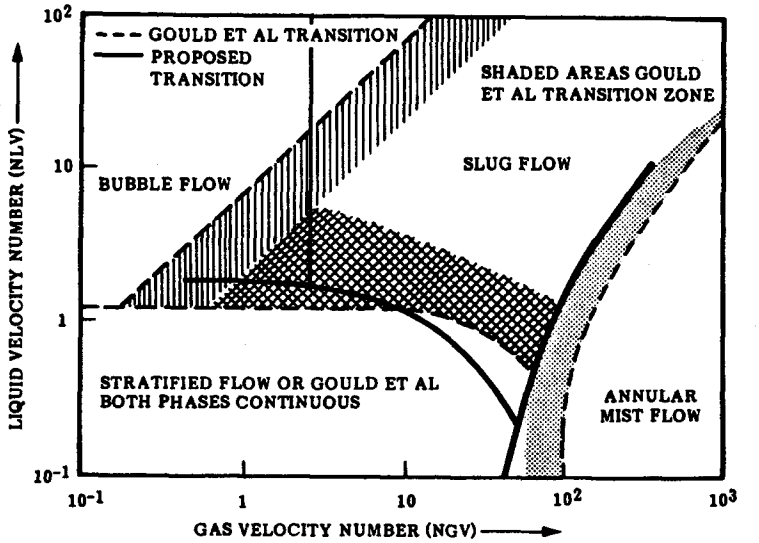

Figure 20. Comparison of proposed flow pattern transition equations with Gould *et al.* map—horizontal flow.

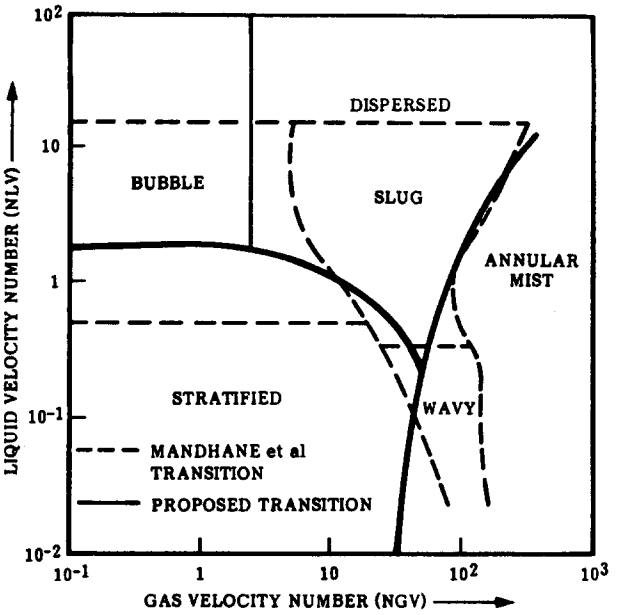

Figure 21. Comparison of proposed flow pattern transition equations with Mandhane *et al.* map—horizontal flow.

numbers just the opposite will happen. The annular mist transition is not affected by the angle of inclination.

Horizontal flow transition predictions were also compared to the Mandhane *et al.* (1974) map in figure 21. The Mandhane superficial velocity coordinates were converted in figure 21 to liquid and gas velocity number coordinates based on their air–water fluid system. Predictions for the bubble–slug transition are at a lower gas rate than shown by Mandhane. The horizontal stratified flow envelope is slightly larger than given by the Mandhane map. However, most of the stratified-wavy flow pattern defined by Mandhane *et al.* falls in the annular mist zone predicted by this work. At high liquid rates, the slug–annular mist boundaries are almost identical. Considering all transition bands in the Mandhane *et al.* map, the predicted map agrees very well, excepting in the stratified-wavy flow regime. The proposed work did not include high enough superficial liquid velocities or liquid velocity numbers to reach the dispersed or froth flow pattern which Mandhane et al predict to occur at superficial liquid velocities near 5 m/s.

CONCLUSIONS

Empirical equations are developed to predict the flow pattern transitions encountered in two-phase flow in inclined pipes. These equations are based on data for a wide range of upflow and downflow angles. Each of these transitions are correlated with the Duns and Ros dimensionless numbers and the angle of inclination. Predictions are compared with the standard published flow pattern maps and are in reasonably good agreement with most maps.

Acknowledgments—The authors acknowledge the help of Atul Arya during data acquisition. Thanks are also expressed to E. R. Pence, Margot Joiner and Ed Merkel for help in preparation of this manuscript. The project was sponsored by members of the Tulsa University Fluid Flow Projects.

REFERENCES

BARNEA, D., SHOHAM, O. & TAITEL, Y. 1982 Flow pattern transition for downward inclined two phase flow; horizontal to vertical. *Chem. Engr. Sci.* **37**, 735–740.

BARNEA, D., SHOHAM, O. & TAITEL, Y. 1982 Flow pattern transition for vertical downward two phase flow. *Chem. Eng. Sci.* **37,** 741–744.

DIXON, W. J. & BROWN, M. B. 1977 Biomedical computer programs, P-series, University of California Press.

DUNS, H., JR. & ROS, N. C. J. 1963 Vertical flow of gas and liquid mixtures in wells. *Proc. 6th World Pet. Cong.*, 451–465.

GOULD, T. L., TEK, M. R. & KATZ, D. L. 1974 Two-phase flow through vertical, inclined or curved pipe. *J. Pet. Tech* **26,** 915–926.

GOVIER, G. W. and AZIZ, K. 1972 *The flow of complex mixtures in pipes.* Van Nostrand Reinhold Co., New York.

GOVIER, G. W. and OMER, M. M. 1962 The horizontal pipeline flow of air-water mixtures. *Can. J. Chem. Engr.* **40,** 93–104.

GRIFFITH, P. and WALLIS, G. B. 1961 Two-phase slug flow. *J. Heat Transfer, ASME,* 307–320.

HUBBARD, M. G. and DUKLER, A. E. 1966 Characterization of flow regimes in horizontal two-phase flow. *Proc. 1966 Heat Transfer and Fluid Mechanics Conf.*, Santa Clara, Calif.

MANDHANE, J. M., GREGORY, G. A. & AZIZ, K. 1974 A flow pattern map for gas liquid flow in horizontal pipes. *Int. J. Multiphase Flow* **1,** 537–553.

MUKHERJEE, H. 1979 An experimental study of inclined two-phase flow. Ph.D. Dissertation, The University of Tulsa.

OSHINOWO, T. & CHARLES, M. E. 1974 Vertical two-phase flow part I. flow pattern correlations. *Can. J. Chem. Eng.* **52.**

SCHMIDT, Z., BRILL, J. P. & BEGGS, H. D. 1981 Experimental study of two-phase normal slug flow in a pipeline-riser pipe system. *J. Ener. Res. Tech.* **103,** 67–75.

TAITEL, Y., BARNEA, D. & DUKLER, A. E. 1980 Modeling flow pattern transitions for steady upward gas–liquid flow in vertical tubes. *AIChE J.* **26,** 3, 345–354.

TAITEL, Y. and DUKLER, A. E. 1976 A model for predicting flow regime transitions in horizontal and near horizontal gas–liquid flow. *AIChE J.* **22,** 1, 47–55.

WALLIS, G. B. 1969 *One dimensional two-phase flow.* McGraw-Hill, New York.